

PAPER • OPEN ACCESS

## Performance of LGAD strip detectors for particle counting of therapeutic proton beams

To cite this article: Vincenzo Monaco *et al* 2023 *Phys. Med. Biol.* **68** 235009

View the [article online](#) for updates and enhancements.

### You may also like

- [4D tracking with ultra-fast silicon detectors](#)  
Hartmut F-W Sadrozinski, Abraham Seiden and Nicolò Cartiglia
- [Measurements of time and spatial resolution of AC-LGADs with different designs](#)  
G. D'Amen, W. Chen, G. Giacomini et al.
- [Signal formation and sharing in AC-LGADs using the ALTIROC 0 front-end chip](#)  
G. D'Amen, W. Chen, C. de la Taille et al.



## PAPER

## Performance of LGAD strip detectors for particle counting of therapeutic proton beams

## OPEN ACCESS

RECEIVED  
4 June 2023REVISED  
11 September 2023ACCEPTED FOR PUBLICATION  
12 October 2023PUBLISHED  
29 November 2023

Original content from this work may be used under the terms of the [Creative Commons Attribution 4.0 licence](#).

Any further distribution of this work must maintain attribution to the author(s) and the title of the work, journal citation and DOI.



Vincenzo Monaco<sup>1,2</sup>, Omar Hammad Ali<sup>3</sup>, Davide Bersani<sup>4</sup>, Mohammed Abujami<sup>1,2</sup>, Maurizio Boscardin<sup>3,5</sup>, Nicolò Cartiglia<sup>2</sup>, Gian Franco Dalla Betta<sup>5,6</sup>, Emanuele Data<sup>1,2</sup>, Marco Donetti<sup>7</sup>, Marco Ferrero<sup>2</sup>, Francesco Ficorella<sup>3</sup>, Simona Giordanengo<sup>2</sup>, Oscar Ariel Marti Villarreal<sup>3</sup>, Felix Mas Milian<sup>1,2,8</sup>, Mohammad-Reza Mohammadian-Behbahani<sup>9</sup>, Diango Montalvan Olivares<sup>1,2</sup>, Marco Pullia<sup>7</sup>, Francesco Tommasino<sup>5,6</sup>, Enrico Verroi<sup>5</sup>, Anna Vignati<sup>1,2</sup>, Roberto Cirio<sup>1,2</sup> and Roberto Sacchi<sup>1,2</sup>

<sup>1</sup> Università degli Studi di Torino, via Pietro Giuria 1, I-10125 Torino, Italy

<sup>2</sup> Istituto Nazionale di Fisica Nucleare, sezione di Torino, Italy

<sup>3</sup> Fondazione Bruno Kessler, Center for Sensors & Devices, Trento, Italy

<sup>4</sup> Istituto Nazionale di Fisica Nucleare, sezione di Pisa, Italy

<sup>5</sup> Trento Institute for Fundamental Physics and Applications, Povo, Trento, Italy

<sup>6</sup> Università degli Studi di Trento, Trento, Italy

<sup>7</sup> CNAO, Centro Nazionale di Adroterapia Oncologica, Pavia, Italy

<sup>8</sup> Universidade Estadual de Santa Cruz, Department of Exact and Technological Sciences, Ilhéus, Brazil

<sup>9</sup> School of Mechanical Engineering, Shiraz University, Shiraz, Iran

E-mail: [monaco@to.infn.it](mailto:monaco@to.infn.it)

**Keywords:** proton therapy, beam monitoring, silicon sensor, particle counting, count-loss correction

## Abstract

**Objective.** The performance of silicon detectors with moderate internal gain, named low-gain avalanche diodes (LGADs), was studied to investigate their capability to discriminate and count single beam particles at high fluxes, in view of future applications for beam characterization and on-line beam monitoring in proton therapy. **Approach.** Dedicated LGAD detectors with an active thickness of 55  $\mu\text{m}$  and segmented in 2  $\text{mm}^2$  strips were characterized at two Italian proton-therapy facilities, CNAO in Pavia and the Proton Therapy Center of Trento, with proton beams provided by a synchrotron and a cyclotron, respectively. Signals from single beam particles were discriminated against a threshold and counted. The number of proton pulses for fixed energies and different particle fluxes was compared with the charge collected by a compact ionization chamber, to infer the input particle rates. **Main results.** The counting inefficiency due to the overlap of nearby signals was less than 1% up to particle rates in one strip of 1 MHz, corresponding to a mean fluence rate on the strip of about  $5 \times 10^7 \text{ p}/(\text{cm}^2 \cdot \text{s})$ . Count-loss correction algorithms based on the logic combination of signals from two neighboring strips allow to extend the maximum counting rate by one order of magnitude. The same algorithms give additional information on the fine time structure of the beam. **Significance.** The direct counting of the number of beam protons with segmented silicon detectors allows to overcome some limitations of gas detectors typically employed for beam characterization and beam monitoring in particle therapy, providing faster response times, higher sensitivity, and independence of the counts from the particle energy.

## 1. Introduction

The adoption of charged particle therapy (CPT) for cancer treatment is rapidly growing worldwide (Durante *et al* 2017, Matsumoto *et al* 2021, Radhe 2022), thanks to its physical and biological advantages over conventional radiotherapy with x-rays for many tumor types. The most advanced dose delivery modalities in CPT are based on pencil beam scanning techniques (Haberer *et al* 1993, Lomax 1999, Lomax *et al* 2004), where the accuracy of the dose distribution is guaranteed by the precise real-time measurement by a beam monitor

device of the number of particles delivered by thousands of pencil beams to the spots in which the tumor is virtually segmented. Dedicated monitoring detectors are also employed to measure online the beam position and profiles. The information from the monitoring system is used to provide fast feedback to the beam delivery and the scanning magnets to assure the dose distribution is the same as foreseen by the Treatment Planning System (Giordanengo *et al* 2015, Paganetti *et al* 2018).

Gas detectors, mainly planar ionization chambers (Lin *et al* 2009, Giordanengo *et al* 2013, Courtois *et al* 2014) or multi-wire proportional chambers (Coutrakon *et al* 1991, Combs *et al* 2010), are typically employed as beam monitors for particle therapy applications, due to their robustness and stability. The main drawbacks are their limited sensitivity (a minimum of a few thousands of protons can be detected by a planar ionization chamber) and slow response due to the long charge collection time (of the order of hundreds of  $\mu\text{s}$  for ions). Future trends in delivery techniques will require faster scanning speeds with the ability to detect a low number of particles delivered to each spot to treat moving targets with rescanning (Klimpki *et al* 2018) or more advanced adaptive methods (Loeffler *et al* 2013).

Different alternative technologies have been investigated to improve the sensitivity, the spatial resolution or the readout speed of conventional gas detectors. Micro-pattern gaseous detectors based on electron multiplier technology (Sauli 1997) allow extending the sensitivity to lower beam currents (Terakawa *et al* 2015, Altieri *et al* 2018). Parallel-plate ionization chambers (IC) with electrodes segmented in strips and optimized for high spatio-temporal resolutions were proposed to monitor the beam profile and beam fluence in treatments with protons at high dose rates (Yang *et al* 2022). Detectors based on multi-layer ribbons of thin scintillator fibers (Leverington *et al* 2018) provide good results in terms of position and lateral width resolutions. However, no above-mentioned proposal provides fluence measurements with a precision comparable with planar ionization chambers. Another limitation of gas detectors and scintillators is that they provide integral signals proportional to the released charge, and the number of delivered particles can be determined only by knowing the nominal beam energy. In addition, gas detectors are not operable in magnetic fields, as required in MRI-guided particle therapies (Hoffmann *et al* 2020), and scintillators suffer from non-linearity effects and poor tolerance to radiation damage.

Planar silicon sensors are promising candidates as beam monitoring detectors. Their sensitivity to single particles allows the direct measurement of the number of delivered particles, regardless of prior knowledge of the beam energy and of the environmental conditions, with a very fast response time. In addition, a low detector thickness and a fine segmentation assure a minimal perturbation of the beam and a very precise spatial resolution. Furthermore, they can be operated in magnetic fields.

Silicon detectors based on flat panels developed for x-ray imaging and depleted monolithic active pixel sensors (DMAPS) were tested with proton beams in charge integration modality (Martišiková *et al* 2011, Flynn *et al* 2022, Dierlamm *et al* 2023). Direct particle counting of proton beams was investigated using the Medipix3 hybrid pixel detector (Yap *et al* 2021). These studies showed very good results for beam profiling, while in general the fluence linearity and resolution were affected by the charge sharing between the small pixels of the detectors or by baseline shifts in case of DMAPS pixel detectors.

In recent years, silicon sensors with a controlled internal charge multiplication mechanism, named Low Gain Avalanche Diodes (LGAD) (Pellegrini *et al* 2014), have been developed and optimized for high-energy physics applications, in particular for their excellent temporal resolution (Sadrozinski *et al* 2018, Cartiglia *et al* 2022). This technology is interesting for particle counting applications, due to the possibility of using thin sensors (active thickness of few tens of  $\mu\text{m}$ ) with signals of very short durations (about 1 ns), allowing to limit the counting inefficiencies at high rates due to the overlap of nearby signals (pile-up). The signal loss due to the reduced thickness is compensated by the internal gain mechanism.

This work describes the performance of LGAD detectors segmented in strips to detect and count protons of the therapeutic beams of the National Centre for Oncological Hadrontherapy (CNAO, Pavia) and the Trento Proton Therapy Center (PTC) in Italy. The counting inefficiencies under high particle rates due to the pile-up effect are mitigated by correction algorithms based on logic correlations of signals from two neighboring channels, extending the counting capability beyond the design goal. The algorithms work also for non-uniform irradiation fields and provide an estimation of the duty cycle of bunched beams. They can be implemented on a digital processing electronics for real-time measurements without adding additional dead time.

The limitations due to the tolerance of these detectors at high radiation doses and future developments toward the use of this technology at nominal therapeutic fluxes ( $10^9$ – $10^{10}$   $\text{s}^{-1} \text{cm}^{-2}$ ) with large-scale panels are also discussed.

## 2. Material and methods

### 2.1. LGAD strip sensors

Low-gain avalanche diode (LGAD) is a manufacturing technology to integrate a moderate and controlled internal charge multiplication mechanism in silicon detectors (Pellegrini *et al* 2014). The charge multiplication

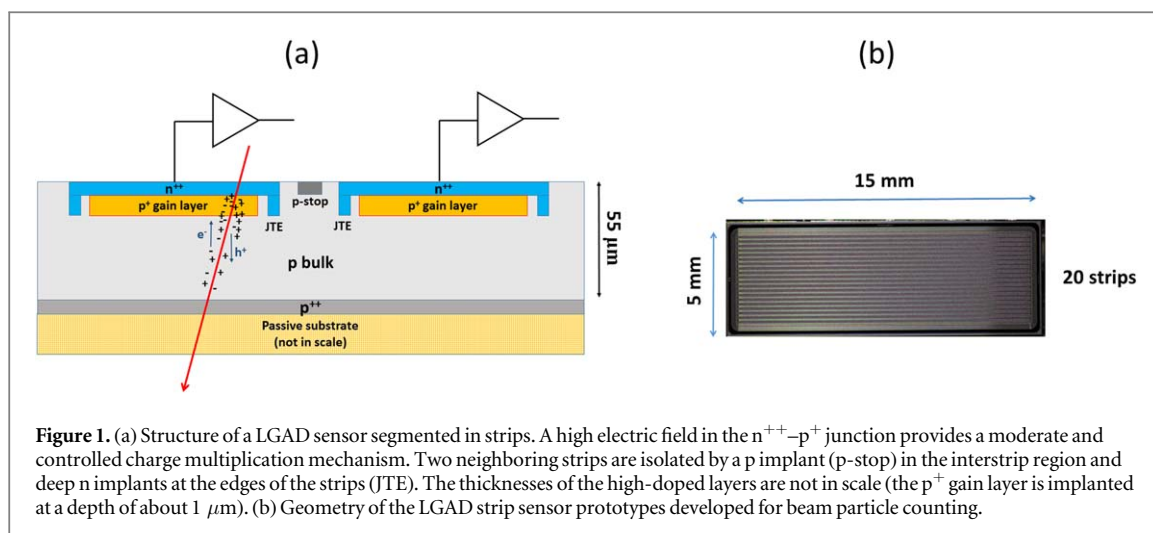


**Figure 1.** (a) Structure of a LGAD sensor segmented in strips. A high electric field in the  $n^{++}$ - $p^+$  junction provides a moderate and controlled charge multiplication mechanism. Two neighboring strips are isolated by a p implant (p-stop) in the interstrip region and deep n implants at the edges of the strips (JTE). The thicknesses of the high-doped layers are not in scale (the  $p^+$  gain layer is implanted at a depth of about  $1 \mu\text{m}$ ). (b) Geometry of the LGAD strip sensor prototypes developed for beam particle counting.

is obtained by implanting an additional acceptor  $p^+$  layer below the  $n^{++}$  readout electrodes of an n-on-p silicon diode; when inversely polarized, a high electric field is formed in the  $n^{++}$ - $p^+$  junction enabling charge multiplication for impact of electrons accelerated in this region (figure 1(a)). The multiplication mechanism provides an enhanced signal, preserving the proportionality with the energy released in the sensor. LGAD detectors are characterized by high time resolutions (about 30 ps) and by a higher signal-to-noise ratio with respect to traditional silicon sensors with the same geometry, allowing to reduce the amplifier gain and the power consumption of the readout electronics.

Dedicated LGAD detectors have been developed within the MoVe-IT<sup>10</sup> project of Istituto Nazionale di Fisica Nucleare (INFN) to investigate their performance as proton counters. They were designed by Fondazione Bruno Kessler (FBK) of Trento, Italy, in collaboration with INFN and included in a wider production of LGAD sensors performed in 2017 by FBK. These sensors have a thickness of the active volume of  $55 \mu\text{m}$  and are segmented in strips of 15 mm length and  $150 \mu\text{m}$  width with a pitch of  $216 \mu\text{m}$  (figure 1(b)). The lateral side of the sensor at the edge of the strips is 5 mm, the active area of each strip, where the  $p^+$  layer is implanted, is  $2 \text{mm}^2$  (corresponding to a strip capacitance of 7 pF). The isolation between two neighboring strips is guaranteed by highly doped p-type implants (p-stop) in the interstrip region and by deep  $n^{++}$  implants (Junction Termination Extension, JTE) at the borders of each strip, which confine the electric field below the active layer (figure 1(a)). The inter-strip region, within which no charge multiplication occurs, has a nominal width of  $66 \mu\text{m}$ . The whole structure is surrounded by guard rings to isolate the detector and collect the leakage current in order to operate the sensor at high bias voltages. From a simulation of the entire structure with TCAD software<sup>11</sup>, it results that no considerable signal is produced by particles hitting the interstrip region and that the probability a particle crossing the edge of a strip induces a signal in the neighboring strip is negligible. The count loss due to pile-up depends on the area of individual strips. For the design signal duration of 1.5 ns, the counting inefficiency in the LGAD strip sensors is expected to be less than 1% up to an input rate of 1 MHz on each strip, corresponding to a fluence rate on the strip<sup>12</sup> of at least  $5 \cdot 10^7 \text{p}/(\text{cm}^2 \cdot \text{s})$ .

The strip sensors were produced in 18 wafers with different doping strategies for the  $p^+$  gain layer to study the optimal design, which maximizes their radiation hardness (Ferrero *et al* 2019). The electrical characterization of the LGAD structures and their radiation resistance were studied independently of this work, with results reported in Sola *et al* (2019). The nominal gain (ratio between the charge produced in the LGAD versus the charge produced in a sensor without the  $p^+$  layer with the same geometry and the same bias voltage) increases with the applied bias voltage, with a typical value at 250 V of 10.

The silicon strip sensors were tested with the therapeutic proton beam of CNAO in May 2018 and of the Trento PTC in July 2019, aiming to study the discrimination and counting capabilities of the detectors.

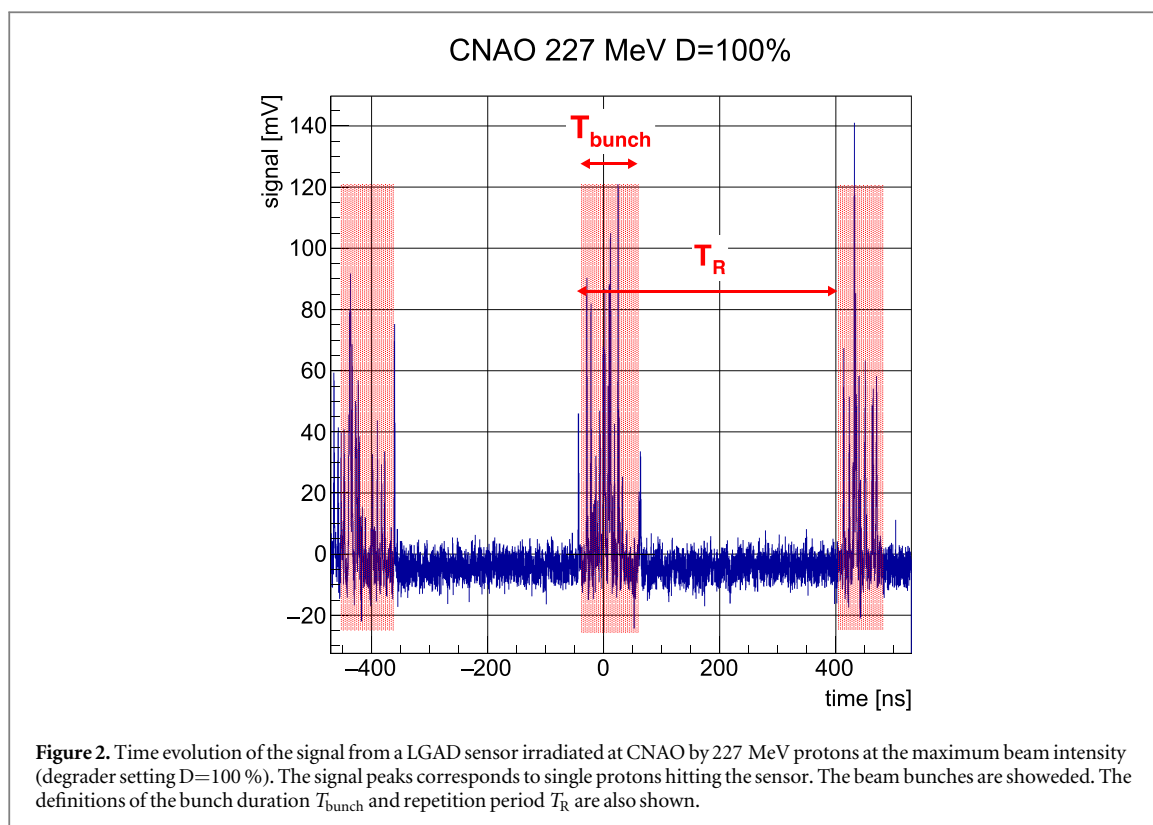
## 2.2. Beam characteristics at CNAO and trento PTC

At CNAO protons are accelerated by a synchrotron at a set of pre-defined energies in the range 60–227 MeV. The beam intensity can be selected at the 100%, 50% and 20% (in the following called ‘degrader setting’) of the

<sup>10</sup> <https://www.tifpa.infn.it/projects/move-it/>

<sup>11</sup> [www.synopsys.com/silicon/tcad.html](http://www.synopsys.com/silicon/tcad.html)

<sup>12</sup> The conversion from count rate to fluence rate on a strip assumes a uniform strip illumination. The estimations are therefore lower limits of the maximum local fluence rate in case of pencil beams covering a fraction of the strip area.



maximum particle rate of  $3.0 \cdot 10^9 \text{ p s}^{-1}$  (Mirandola *et al* 2015). Periodic delivery phases, called spills, of about 1 second duration, are followed by inter-spill periods during which particles are accumulated and accelerated. Inside each spill, particles are delivered in bunches synchronous with the revolution period  $T_R$  of the accelerator. As an example of the time distribution of the CNAO beam, figure 2 shows the signal from a LGAD sensor irradiated by 227 MeV protons at the maximum beam intensity: the peaks correspond to single protons hitting the sensor and single bunches are shadowed. Under the assumption of regular bunches of duration  $T_{\text{bunch}}$ , the duty cycle is defined as  $\text{DC} = T_{\text{bunch}}/T_R$ .

At the Trento PTC, an IBA ‘Proteus 235’ cyclotron is used to accelerate the beam at a fixed energy of 228 MeV. An energy selection system based on a degrader and magnetic energy selectors is employed to provide the particle beam at the desired energy (down to a minimum of 70 MeV) to the treatment or experimental rooms. The beam particle rate depends on the cyclotron extraction current and on the beam energy, ranging from  $3.8 \times 10^6 \text{ p s}^{-1}$  at 70 MeV, to  $2.3 \times 10^8 \text{ p s}^{-1}$  at 228 MeV for a current of 1 nA. The extraction current can be increased up to 320 nA, and the corresponding particle rate scales accordingly. The extraction current is modulated by a 50% duty-cycle square wave with a 100 ms period. Inside each irradiation period of 50 ms, the particles are delivered synchronous with a fixed phase of the cyclotron radio-frequency (RF), having a period of 9.4 ns (Tommasino *et al* 2017).

The main characteristics of the proton beams of CNAO and Trento PTC, summarized in table 1, reflect the typical values for therapeutic proton beams provided by synchrotrons and cyclotrons, respectively.

### 2.3. Experimental setup

For the tests with proton beams, the strip sensors were mounted on a passive custom board, used to distribute the high voltage to the sensor and feed the signal from two channels to external amplifiers. An example is shown in figure 3, where two sensors were mounted on the board and the signals from two neighboring strips of one sensor were fed to external 40 dB high bandwidth (2.5 GHz) amplifiers (Cividec C2<sup>13</sup>) through SMA connectors, while the other strips and the guard ring were grounded. The bias voltage was provided by an external power supply (CAEN DT1570<sup>14</sup>). The amplified signals were collected by a 5 GSa/s 500 MHz bandwidth digitizer (CAEN DT5742<sup>15</sup>), controlled by a PC through an optical connection. The digitizer acquisition was managed by a dedicated CAEN software, which collected and stored waveforms of 1024 samples and 204.8 ns duration in

<sup>13</sup> <https://cividec.at/electronics-C2-HV.html>

<sup>14</sup> <https://www.caen.it/products/dt1470et/>

<sup>15</sup> <https://www.caen.it/products/dt5742/>

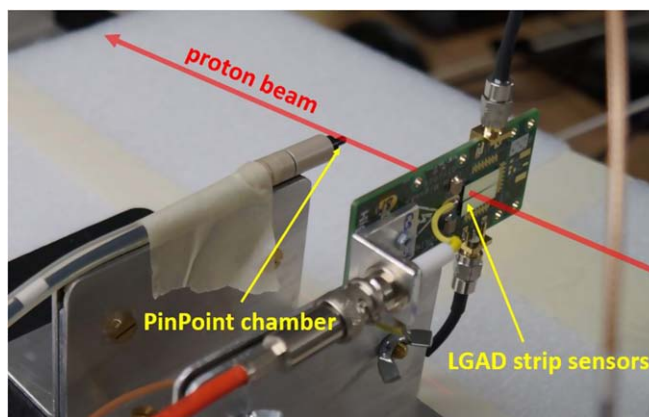


**Figure 3.** Two strip sensors mounted on a custom HV-distribution board and a compact ionization chamber aligned along the beam direction. The same setup was employed at CNAO and at the Trento PTC.

**Table 1.** Main specifications of the proton beams at CNAO and at Trento PTC.

	CNAO	Trento PTC
Energy range	60–227 MeV	70–228 MeV
Beam particle rate	$D \times 3.0 \cdot 10^9 \text{ p s}^{-1}$ $D = 100\%, 50\%, 20\%$	$3.8 \times 10^6$ (1 nA)— $1.1 \times 10^9 \text{ p s}^{-1}$ (320 nA) at minimum energy $2.3 \times 10^8$ (1 nA)— $7.4 \times 10^{10} \text{ p s}^{-1}$ (320 nA) at maximum energy
Beam range for protons	3–32 g cm <sup>-2</sup> from lowest to highest energy	4–32 g cm <sup>-2</sup> from lowest to highest energy
FWHM in air of spot at the isocenter	7–20 mm from highest to lowest energies	6–16 mm from highest to lowest energies
Field size	20 × 20 cm <sup>2</sup>	max 30 × 40 cm <sup>2</sup>

correspondence with asynchronous software triggers. The samples were digitized with 12 bits, 1 ADC count corresponding to 0.244 mV. The conversion time of the digitizer (110  $\mu\text{s}$ ) and the time needed to transmit and store the data ( $\sim 500 \mu\text{s}$ ) limited the acquisition rate to about 1 kHz and the acquisition efficiency to  $3 \times 10^{-4}$ . All the instruments and the acquisition data-flow were controlled from the control room through Ethernet connection.

In both the tests at CNAO and at the Trento PTC, a compact ionization chamber (IC) was aligned with the beam and positioned behind the readout strips, as shown in figure 3. A PinPoint PTW T31015<sup>16</sup> chamber with a volume of 0.03 cm<sup>3</sup> and a PTW Unidos electrometer<sup>17</sup> were used at CNAO. At Trento a IBA CC01<sup>18</sup> chamber with a cavity volume of 0.01 cm<sup>3</sup> and the electrometer model ‘Dose 1’ from IBA were used. In the offline analysis, the IC measurements were correlated to the count rates of the LGAD strips to provide an estimation of the input particle rate in one strip. It should be remarked that, given the different areas covered by the IC and the strips, such correlations depend on the beam transversal shape, which changes with the beam energy.

At CNAO the sensor was positioned at the isocenter and irradiated by a proton beam kept at a fixed position with three different energies: 62, 110 and 227 MeV. For each energy, three runs were acquired, with degrader settings of 100%, 50% and 20%. For each run, a pre-defined number of spills, between 10 and 30, depending on the beam energy and degrader setting, were delivered, in order to reach a statistical error of about 1% in the number of discriminated signals from the LGAD strip. For each irradiation, the signals from two neighboring strips were collected by the digitizer. In parallel, the integral charge produced in the compact IC positioned behind the strips was registered for each acquisition run.

In the offline analysis, individual beam particles were discriminated over the background noise and counted. The number of signals from each strip was converted to a count rate using the total duration of the acquired waveforms. The total acquisition time did not include inter-spill periods, vetoed in the acquisition by an external signal provided by the accelerator control system. Likewise, the charge produced in the electrometer was

<sup>16</sup> <https://www.ptwdosimetry.com/en/products/pinpoint-ion-chambers-31014–31015/>

<sup>17</sup> <https://www.ptwdosimetry.com/en/products/unidos-e/>

<sup>18</sup> <https://www.iba-dosimetry.com>

converted to a charge rate averaged over the irradiation time, by using a time stamp saved in the digitizer output files, which allows to determine the duration of the irradiation with a precision of 1 ms.

The beam test at the experimental room of the Trento PTC was performed using the same setup employed at CNAO, except for the compact IC (IBA CC01 at Trento) and the units reported by the electrometer used to readout the chamber (mGy at Trento, nC at CNAO). In both cases, a linearity of the electrometer output with the number of delivered particles was assumed for each fixed beam energy, to estimate the input particle rate, as described in sections 3.2 and 3.4. The sensors were irradiated by protons at four different energies (70, 125, 179, 228 MeV), with the pencil beam, the sensor and the compact chamber in fixed relative positions. For each energy, several runs (between 5 and 9) were collected with different cyclotron currents corresponding to particle rates in one strip between 0.5 MHz and a few MHz. The duration of each run was such to keep the statistical error on the number of counts from each strip below 1%.

## 2.4. Count-loss corrections

The data collected during the beam tests were analyzed to identify and count single protons, whose signals exceed a predefined threshold. However, signals too close in time cannot be separated, causing a counting inefficiency, which gets worse with the particle rate. Two algorithms, named ‘two-channel time combination’ (TC) and ‘two-channel count combination’ (CC) methods, described in Mohammadian-Behbahani *et al* (2022), were developed to correct for counting inefficiencies, even when the irradiation is not continuous. The algorithms are based on the logic combinations of logical signals from two independent detectors, where the logical signals from each channel are assumed to be generated at the discrimination stage with a duration equal to the system dead time.

In the CC method, the number of signals from the two channels ( $N_1$  and  $N_2$ ) and the number of transitions of their logic OR ( $N_{OR}$ ) are counted in a given acquisition time ( $T_{acq}$ ). The CC method estimates the particle rates in the two channels corrected for pile-up effects, as:

$$f_{in,1} = \frac{(k+1)f_{m,1}f_{m,2}}{kf_{m,OR}} \quad (1a)$$

$$f_{in,2} = kf_{in,1}, \quad (1b)$$

where  $f_{m,X} = N_X/T_{acq}$  (with  $X = 1, 2, OR$ ) are the measured count rates. The factor  $k$  in equations (1a) and (1b) is the ratio of the input rates in the two channels (for example due to different geometrical acceptances), which is assumed either to be known in advance, or can be estimated from measurements at low-rate conditions, where pile-up effects are negligible. In the application of the correction method to the data collected at CNAO and at the Trento PTC, a  $k$  factor equal to 1 was assumed, justified by the observation that the difference in the average number of counts from two neighboring strips was less than 1%.

The TC method is based on the measurement of the durations of the single logical pulses from the two channels ( $T_1$  and  $T_2$ ) and of their AND logic combination ( $T_{AND}$ ). The pile-up corrected input particle rates for the two channels are given by:

$$f_{in,1} = \frac{f_{m,1}}{1 - \frac{T_{AND}}{T_2}} \quad (2a)$$

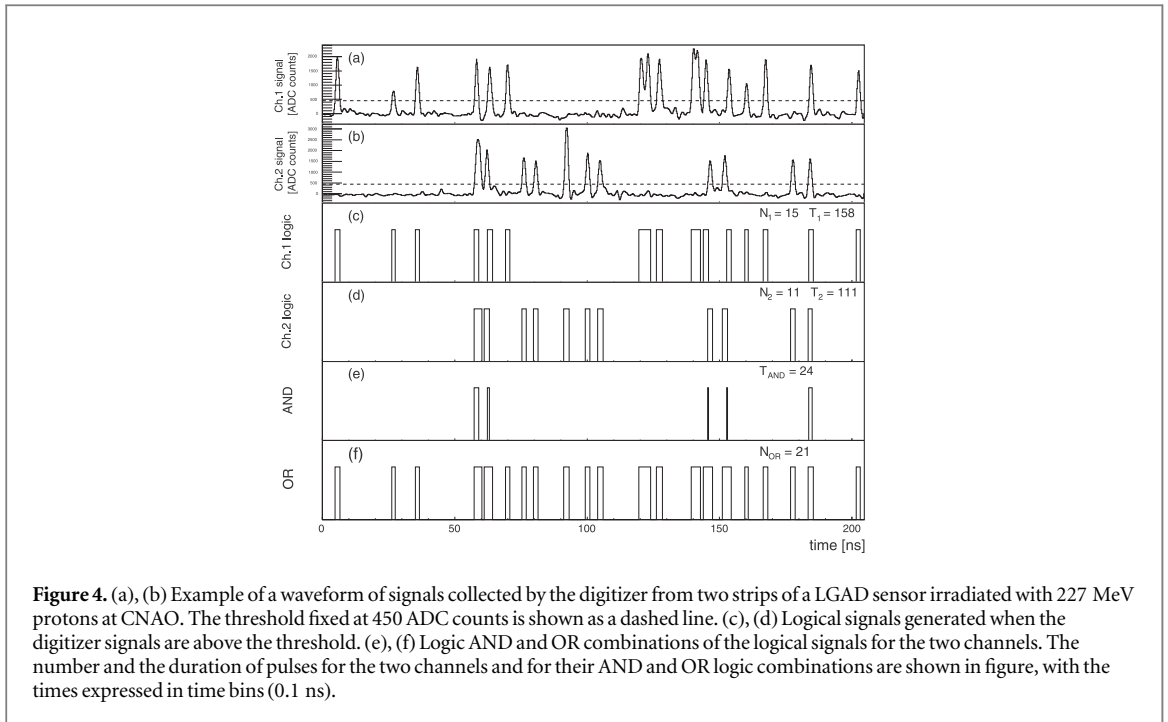
$$f_{in,2} = \frac{f_{m,2}}{1 - \frac{T_{AND}}{T_1}}. \quad (2b)$$

The counting and the logic needed for the pile-up corrections are easily implementable on digital processing electronics for real-time operations, without additional dead time. Both the algorithms were validated with simulations of random pulses in ideal conditions (absence of noise, no charge sharing between the two channels and perfect detection efficiency), and were proven to be able to correct for inefficiency effects without any *a priori* knowledge of the system dead time and independently of the detail of the dead-time model (Mohammadian-Behbahani *et al* 2022). In the current study, the signal waveforms collected simultaneously by two LGAD strips are analyzed to check the performance of the correction algorithms in a more realistic situation.

For the signals provided by a silicon sensor, it can be reasonably assumed that the system follows a paralyzable (extendable) dead-time model (Knoll 2010), where the measured count rate  $f_m$  is related to the input event rate  $f_{in}$  by:

$$f_m = f_{in} \cdot e^{-\tau f_{in}}. \quad (3)$$

The comparison between the measured count rates and the input rates estimated by equations (1) or (2) allows to determine, for each measurement, the system dead time  $\tau$ , by inverting equation (3).



For a continuous beam, where the particle flux is constant, the dead time  $\tau$  in equation (3) is equal to the intrinsic system dead time  $\tau_o$ , given by the average signal duration. For non-continuous radiation sources, like the bunched beams of CNAO, the count rates in equations (1) and (2) are values averaged over all the acquisition time, while the counting inefficiency depends on the instantaneous input rate in each bunch.

If the time distribution of the input particles can be described as regular bunches whose duration is a fraction DC (duty cycle) of the full irradiation period, and assuming a constant input rate inside each bunch, the dead time  $\tau$  in equation (3) is related to the intrinsic system dead time  $\tau_o$  by:

$$\tau = \frac{\tau_o}{DC}. \quad (4)$$

The knowledge of the intrinsic dead time  $\tau_o$  allows to estimate the duty-cycle DC of the bunches or, equivalently, the instantaneous input particle rate  $f_{in}^{inst}$ :

$$f_{in}^{inst} = \frac{f_{in}}{DC}, \quad (5)$$

where  $f_{in}$  is obtained from equations (1) or (2).

In case of pulsed sources, like at the Trento PTC, where the particles are emitted in very short packets with duration less than  $\tau_o$  and with a repetition frequency  $f_R$  synchronous with the cyclotron RF, it can be demonstrated that, for  $f_{in}/f_R \ll 1$ , the dead time is:

$$\tau \approx T_R. \quad (6)$$

### 3. Results

#### 3.1. Discrimination of LGAD proton signals

An example of a digitizer waveform collected at CNAO by two strips of a LGAD sensor irradiated with 227 MeV protons is shown in figures 4(a), (b). The peaks correspond to signals from individual protons, which can be separated from the background noise by discriminating them against a fixed threshold (dashed line). In some cases, signals close in time are overlapped. The duration of an individual signal is about 2 ns, compatible with the expected charge collection time (1.5 ns for these sensors) and with the 500 MHz bandwidth of the digitizer. Each signal is followed by baseline oscillations, whose amplitudes are in general below the threshold used to discriminate particle signals. The input signals were linearly interpolated to double the data points, and two data-flows of logical signals were generated with logical 1 when the signal samples were above the threshold (figures 4(c), (d)). In order to apply the pile-up correction algorithms described in section 2.4, the two logical data-flows were combined with AND and OR logics (figures 4(e), (f)) and the number of digital pulses and their



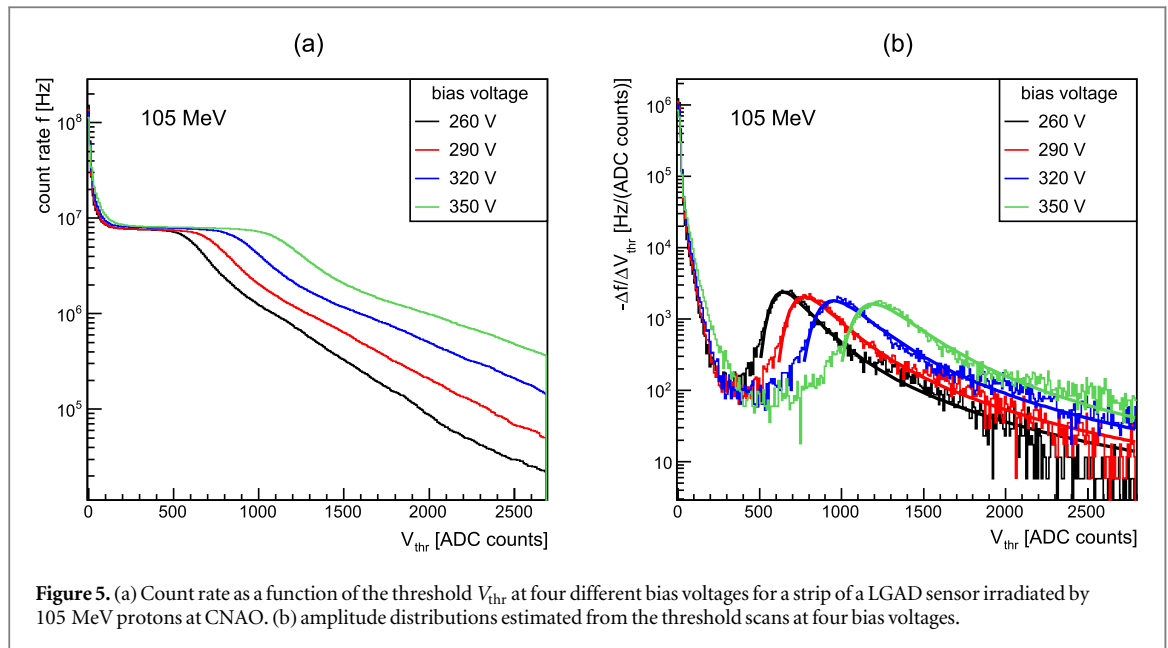


**Figure 5.** (a) Count rate as a function of the threshold  $V_{thr}$  at four different bias voltages for a strip of a LGAD sensor irradiated by 105 MeV protons at CNAO. (b) amplitude distributions estimated from the threshold scans at four bias voltages.

durations were measured for each channel and for their logic combinations, and integrated over all the waveforms collected for each data acquisition.

In order to define an optimal threshold to separate signals from the background, the amplitude distributions were extracted by counting the number of logical pulses as a function of the threshold voltage  $V_{thr}$  (threshold scan). As an example, figure 5(a) shows the count rate for a strip irradiated by 105 MeV protons at CNAO, as a function of  $V_{thr}$  for different bias voltages. The corresponding amplitude distributions, shown in figure 5(b), were estimated as the negative of the discrete derivatives of the threshold scan curves. At low  $V_{thr}$  values, a high number of counts is triggered by the random fluctuations of the baseline level, mainly due to the amplifier intrinsic noise of 2.5 mV rms. The noise amplitude distribution, corresponding to the first part of figure 5(b), drops rapidly by increasing the threshold voltage. The particle signal distribution at higher voltages follows a Landau distribution, well separated from the noise. The most probable value (MPV) of the Landau distribution increases with the bias voltage, due to the increase of the electric field in the  $p^+$  layer, producing an enhanced charge multiplication in the gain region and higher signal to noise ratio.

In both the tests at CNAO and Trento PTC, the sensor was operated at a bias voltage of 350 V. The distributions of the signal amplitudes obtained at CNAO by a threshold scan are shown in figure 6 for three different proton energies, together with the result of fits by a Landau function. A common threshold was chosen as 450 ADC counts (corresponding to 84 mV) for an optimal separation of signals from noise, independent of the beam energy. The same analysis was performed with the data collected at the Trento PTC, providing similar results.

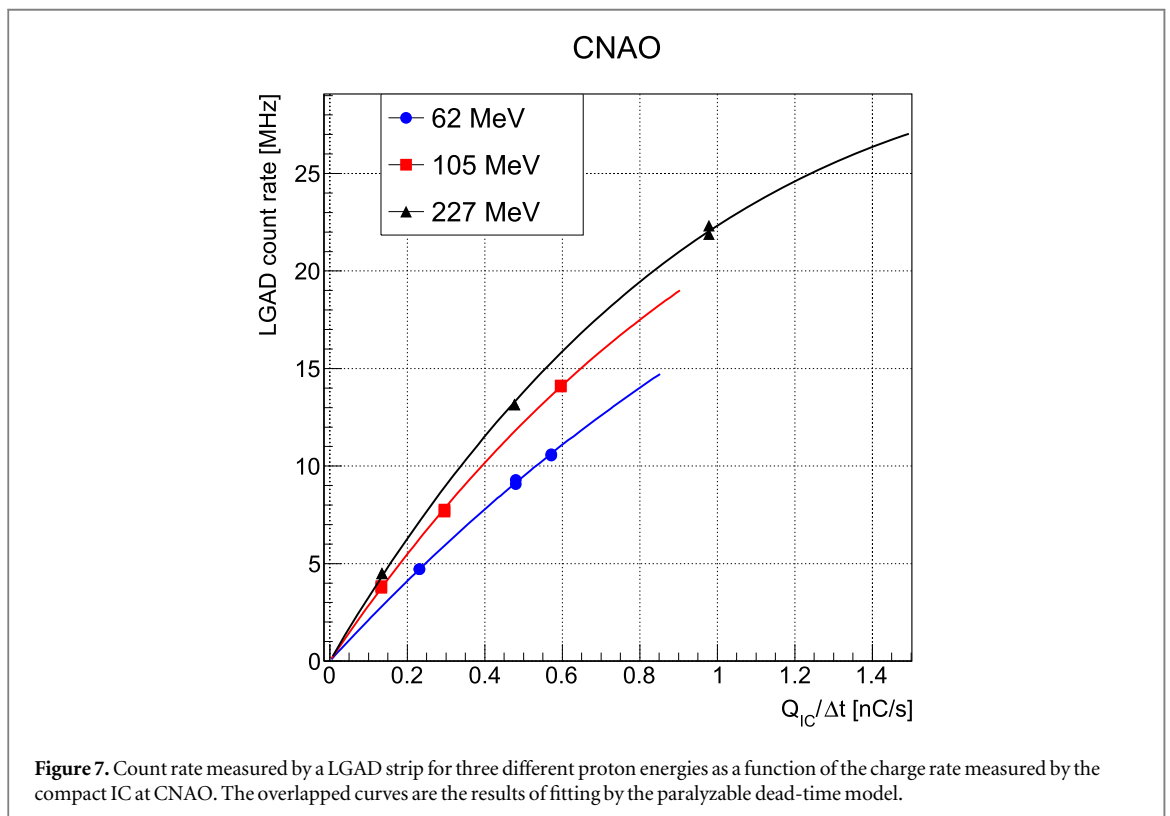
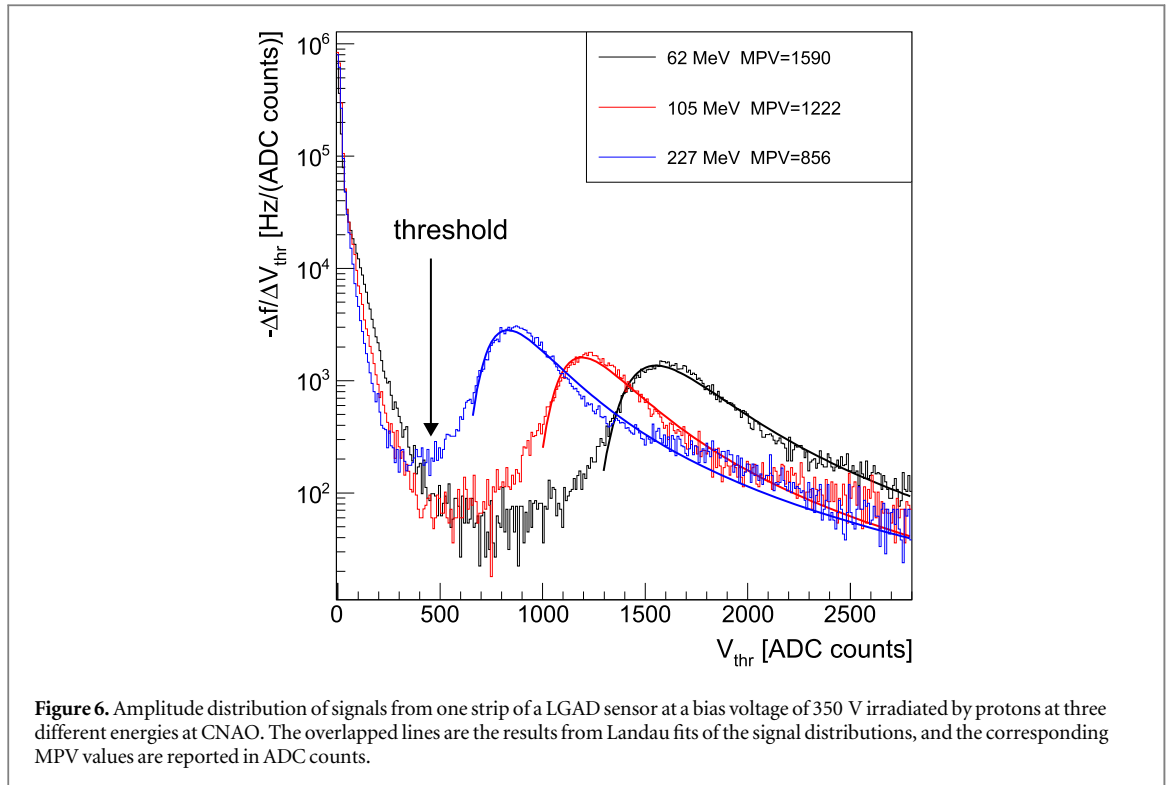
### 3.2. Counting efficiency of LGAD strip sensors (CNAO)

Figure 7 shows the measured count rates in one strip as a function of the charge rate measured with the compact IC, separately for three beam energies. The count rates in the second strip were found to differ on average by less than 1%. In order to parameterize the count inefficiency and estimate the input particle rate in one strip, an extendable (paralyzable) dead-time model is assumed, according to equation (3). The input particle rate in one strip is parameterized as:

$$f_{in} = Q/(C \cdot \Delta t), \quad (7)$$

where  $Q/\Delta t$  is the charge rate measured by the PinPoint IC, and  $C$  is the mean charge produced in the IC by each particle impinging on the readout strip. In the above parameterization it is assumed that, at a fixed energy, the IC output is proportional to the number of particles crossing the IC and to the number of particle crossing the strip; these assumptions are justified by the small recombination effects expected in the small gas volume of the compact IC, on the fixed relative position of the IC and the readout strip and on the independence of the beam transversal shape from the beam flux at each given energy. It is also assumed that the beam time structure does not depend on the degrader settings for a fixed energy.

For each beam energy, the points in figure 7 were fitted by equations (3) and (7), separately for each beam energy, with the dead time  $\tau$  and the parameter  $C$  as free parameters of the fit. The values of the parameters  $\tau$  and  $C$  for each beam energy are reported in table 2.



The C factor decreases as the beam energy increases, as expected by the decrease of the stopping power of protons in the IC gas. The dead times  $\tau$  estimated by fitting are larger than the intrinsic dead time  $\tau_0$  related to the signal duration (given by the signal duration of about 2 ns), because of the bunched structure of the beam, leading to a larger pile-up probability than for a uniform time distribution of the delivered particles with the same average rate. A more detailed study of the bunch structure of the CNAO beam follows in section 3.3.

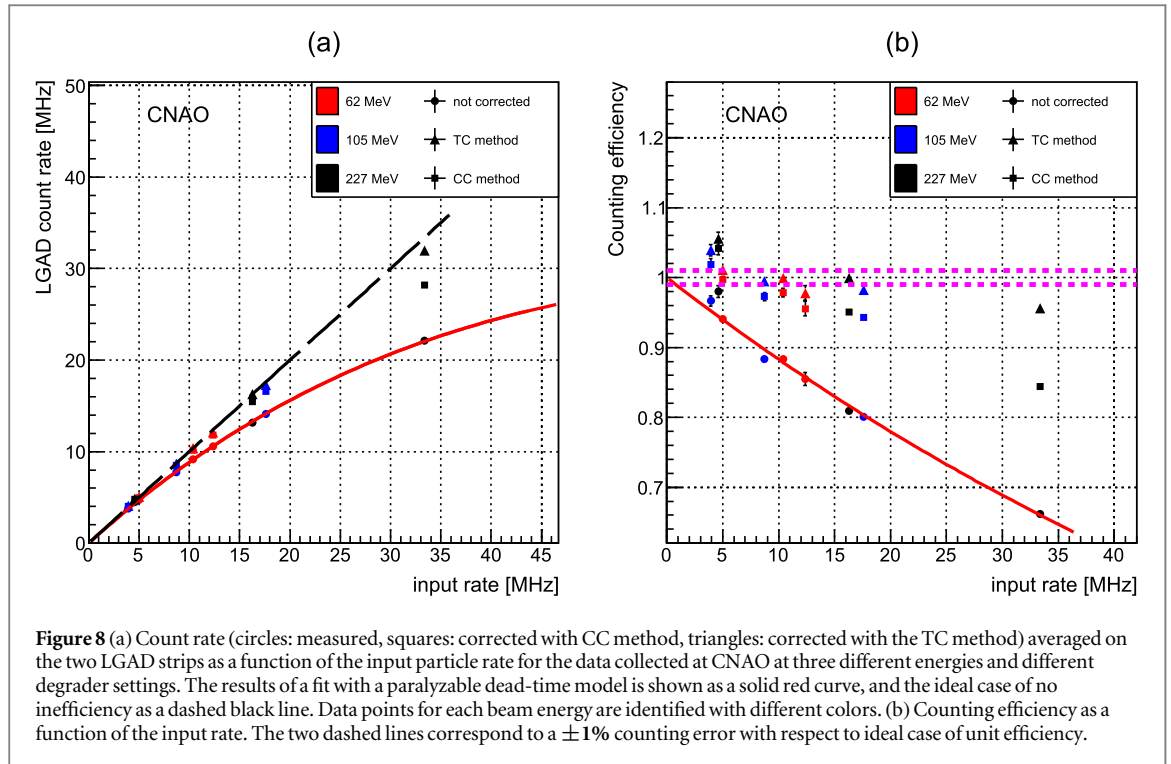


**Table 2.**  $\tau$  and C parameters extracted by fitting the count rate curves by a paralyzable dead-time model at three CNAO energies.

Energy (MeV)	$\tau$ (ns)	C (fC)
62	$12 \pm 1$	$0.0463 \pm 0.0004$
105	$12.7 \pm 0.4$	$0.0338 \pm 0.0003$
227	$12.4 \pm 0.1$	$0.0293 \pm 0.0002$

Once the normalization factor C was determined for each energy, the charge rates measured with the IC in each acquisition run were converted to mean input particle rates hitting the strip, using equation (7). Figure 8(a) shows the count rates measured in the LGAD strip (circles) and the count rates corrected for pile-up inefficiencies with the TC method (triangles) and the CC method (squares), as a function of the estimated input rate. The solid red curve in figure 8(a) is the result of a fit by equation (3), and the dashed black line the ideal behavior without inefficiency effects. The results in figure 8(a) include all the 9 runs of this study, and, for each run, the count rate was averaged over the two readout strips. The same results are shown in figure 8(b) in terms of counting efficiency ( $f_m/f_{in}$ ) as a function of the input count rate  $f_{in}$ .

According to the results of the fit reported in figure 8, the counting error without corrections is less than 1% for  $f_{in} < 1$  MHz, corresponding, for a nominal strip area of  $2 \text{ mm}^2$ , to a mean local fluence rate of  $5 \times 10^7 \text{ p}/(\text{cm}^2 \cdot \text{s})$ . The pile-up correction algorithms show a reasonable performance for particle rates on one strip below 10 MHz, corresponding to a fluence rate on the strip of  $5 \times 10^8 \text{ p}/(\text{cm}^2 \cdot \text{s})$ , well beyond the design goal. However, the results after the correction are in general outside the  $\pm 1\%$  error band. This is probably due to the dependence of the beam time structure on the degrader setting, which affects the input rate estimation, as discussed in the following section. The TC correction algorithms provide count rates higher than the CC method, especially for the three higher input frequencies in figure 8.

It is worth remarking that the input frequency on the horizontal axis of figure 8 is an estimation of the input particle rate averaged over the spill irradiation period, while the pile-up probability and counting inefficiency depend on the instantaneous rate.

### 3.3. Study of the bunched structure of the CNAO beam

An independent measurement of the instantaneous particle rate in one strip can be obtained from the distribution of the time intervals between two consecutive signals which, for a uniform random particle time distribution in a bunch, follows an exponential behavior with a time constant equal to the inverse of the instantaneous particle rate inside the bunch. An example is shown in figure 9, where the distributions of the time

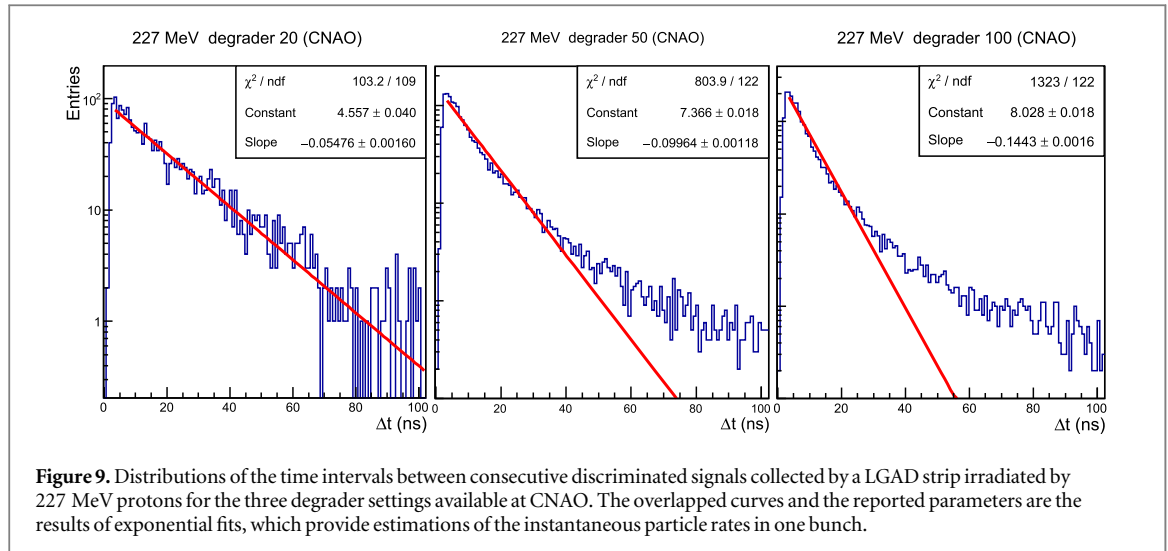


**Figure 9.** Distributions of the time intervals between consecutive discriminated signals collected by a LGAD strip irradiated by 227 MeV protons for the three degrader settings available at CNAO. The overlapped curves and the reported parameters are the results of exponential fits, which provide estimations of the instantaneous particle rates in one bunch.

intervals between two consecutive signals from one strip irradiated by a 227 MeV proton beam at CNAO at the three different degrader settings are fitted by an exponential, providing the instantaneous input frequencies. The fits are restricted to time intervals below 102 ns, limited by the duration of the digitizer waveform of 204 ns. Therefore, frequency components of the beam time distributions lower than few MHz are not evaluated in this study.

It is worth noting that the duration of the digitizer waveforms is lower than the bunch repetition time at CNAO, and therefore it was not possible to study the structure of the CNAO beam using the time evolution of the LGAD signals with the collected data samples. However, the correction algorithms applied to mitigate counting inefficiencies give indication on the bunch structure of the beam, using only the counting measurements from the LGAD strips, as described in section 2.4. In particular, the comparison between the measured count rate  $f_m$  and the count rates corrected by the TC or CC methods can be used to estimate the system dead time  $\tau$  by inverting equation (3), under the hypothesis of a paralyzable dead-time model. Assuming a simplified bunched time structure for the beam, with the particles delivered during a fraction DC of the irradiation time with a constant frequency inside each bunch, the bunch duty cycle DC can be evaluated by comparing the system dead time  $\tau$  with the intrinsic dead time  $\tau_o$ , equal to the time the signal is above threshold, through equation (4). The instantaneous particle rate inside a bunch can therefore be estimated as  $f_{\text{inst}} = f_{\text{corr}} / \text{DC}$ , where  $f_{\text{corr}}$  is the input frequency averaged over the entire irradiation period after the application of the correction algorithms.

Table 3 shows, for each beam energy and degrader setting, the duration of the signal over threshold ( $\tau_o$ ), the  $\tau$  values extracted with the CC method using equation (3) ( $\tau_{\text{CC}}$ ), the corresponding DC values obtained with equation (4) ( $\text{DC}_{\text{CC}}$ ), the average input rate estimated by the CC method ( $f_{\text{corr,CC}}$ ), the instantaneous input particle rates in one strip from equation (5) ( $f_{\text{in,CC}}^{\text{inst}}$ ), to be compared with the input particle rates evaluated from an exponential fitting of the time interval distributions ( $f_{\text{in,fit}}^{\text{inst}}$ ). The results obtained by the TC method are reported in table 4.

It is evident, by comparing in table 3 the instantaneous frequencies obtained from the CC correction method ( $f_{\text{in,CC}}^{\text{inst}}$ ) with the same quantities from the exponential fit ( $f_{\text{in,fit}}^{\text{inst}}$ ), that the CC method provides a good estimation of the beam instantaneous particle rate, excluding the lower degrading setting where it is underestimated. This could be caused by low frequency components of the beam time distribution that are not included in the fitting performed to estimate the instantaneous input particle rate from the time interval distribution, or by the random sampling of the bunch period. The TC method provides higher values for the instantaneous rates, especially at the higher degrading settings at 227 MeV.

As a consequence of the bunched structure of the beam with a DC in the range of 10 to 22%, the instantaneous particle rate within a bunch in each LGAD strip ( $f_{\text{in}}^{\text{inst}}$ ) is a factor between 5 and 10 higher than the average input rate corrected for inefficiency effects ( $f_{\text{corr}}$ ).

In general, it can be observed from tables 3 and 4 that the bunch duty cycle DC increases with the beam flux, indicating that the extraction mechanism provides shorter bunches at lower degrader settings. Based on this study, there is also evidence of a dependence of the bunch structure on the beam energy, for a fixed degrader value. The dependence of DC on the degrader setting partially affects the estimation of the average input particle rate obtained by the fits shown figure 8, which assume that the bunch structure for a given energy does not depend on the particle input rate. The disagreement of the first two corrected frequencies in figure 8 with respect

**Table 3.** Intrinsic dead time ( $\tau_o$ ), estimated effective dead time ( $\tau_{CC}$ ), bunch duty cycle ( $DC_{CC}$ ), average input rate estimated by the CC method ( $f_{corr,CC}$ ), instantaneous input rate estimated by the CC method ( $f_{in,CC}^{inst}$ ) and by an exponential fitting of the time interval distribution between consecutive pulses ( $f_{in,fit}^{inst}$ ), for different beam energies and degrader settings at CNAO.

Energy (MeV)	Degrader	$\tau_o$ (ns)	$\tau_{CC}$ (ns)	$DC_{CC}$ (%)	$f_{corr,CC}$ (MHz)	$f_{in,CC}^{inst}$ (MHz)	$f_{in,fit}^{inst}$ (MHz)
62	20	$2.08 \pm 0.02$	$12 \pm 1$	$18 \pm 2$	$4.99 \pm 0.02$	$28 \pm 3$	$33.8 \pm 0.6$
62	50		$10.0 \pm 0.8$	$21 \pm 2$	$10.2 \pm 0.06$	$49 \pm 4$	$51 \pm 1$
62	100		$9 \pm 1$	$22 \pm 3$	$11.8 \pm 0.1$	$54 \pm 7$	$59 \pm 2$
105	20	$1.94 \pm 0.03$	$13 \pm 3$	$14 \pm 3$	$4.08 \pm 0.03$	$28 \pm 6$	$40 \pm 1$
105	50		$11.4 \pm 0.9$	$16 \pm 1$	$8.49 \pm 0.05$	$51 \pm 4$	$57 \pm 1$
105	100		$9.8 \pm 0.3$	$19.4 \pm 0.6$	$16.60 \pm 0.07$	$86 \pm 3$	$81 \pm 1$
227	20	$1.72 \pm 0.04$	$12 \pm 2$	$13 \pm 2$	$4.78 \pm 0.04$	$38 \pm 7$	$55 \pm 2$
227	50		$10.4 \pm 0.3$	$15.6 \pm 0.5$	$15.47 \pm 0.06$	$99 \pm 3$	$100 \pm 1$
227	100		$8.6 \pm 0.1$	$18.8 \pm 0.3$	$28.2 \pm 0.1$	$150 \pm 3$	$144 \pm 2$

**Table 4.** Intrinsic dead time ( $\tau_o$ ), estimated effective dead time ( $\tau_{TC}$ ), bunch duty cycle ( $DC_{TC}$ ), average input rate estimated by the TC method ( $f_{corr,TC}$ ), instantaneous input rate estimated by the TC method ( $f_{in,TC}^{inst}$ ) and by an exponential fitting of the time interval distribution between consecutive pulses ( $f_{in,fit}^{inst}$ ), for different beam energies and degrader settings at CNAO.

Energy (MeV)	Degrader	$\tau_o$ (ns)	$\tau_{TC}$ (ns)	$DC_{TC}$ (%)	$f_{corr,TC}$ (MHz)	$f_{in,TC}^{inst}$ (MHz)	$f_{in,fit}^{inst}$ (MHz)
62	20	$2.08 \pm 0.02$	$14 \pm 1$	$14 \pm 1$	$5.06 \pm 0.02$	$35 \pm 3$	$33.8 \pm 0.6$
62	50		$11.8 \pm 0.8$	$17 \pm 1$	$10.38 \pm 0.06$	$59 \pm 4$	$51 \pm 1$
62	100		$11 \pm 1$	$19 \pm 2$	$12.1 \pm 0.1$	$65 \pm 7$	$59 \pm 2$
105	20	$1.94 \pm 0.03$	$18 \pm 2$	$11 \pm 2$	$4.08 \pm 0.03$	$38 \pm 5$	$40 \pm 1$
105	50		$13.7 \pm 0.9$	$13.9 \pm 0.9$	$8.68 \pm 0.05$	$63 \pm 4$	$58 \pm 1$
105	100		$11.8 \pm 0.3$	$16.1 \pm 0.4$	$17.30 \pm 0.06$	$108 \pm 3$	$81 \pm 1$
227	20	$1.72 \pm 0.04$	$15 \pm 3$	$10 \pm 2$	$4.85 \pm 0.04$	$46 \pm 7$	$55 \pm 2$
227	50		$13.0 \pm 0.3$	$12.5 \pm 0.3$	$16.26 \pm 0.06$	$130 \pm 3$	$100 \pm 1$
227	100		$11.5 \pm 0.1$	$14.1 \pm 0.2$	$31.9 \pm 0.1$	$227 \pm 3$	$144 \pm 2$

to the expected input particle rate could be due to a wrong estimation of the input particle rate due to this assumption. There was no previous study on the bunch structure of the CNAO beam at the time scale of our study. Further studies will be needed in the future to understand better the fine temporal structure of the CNAO beam and to correlate it with the accelerator settings.

### 3.4. Counting efficiency at the Trento PTC

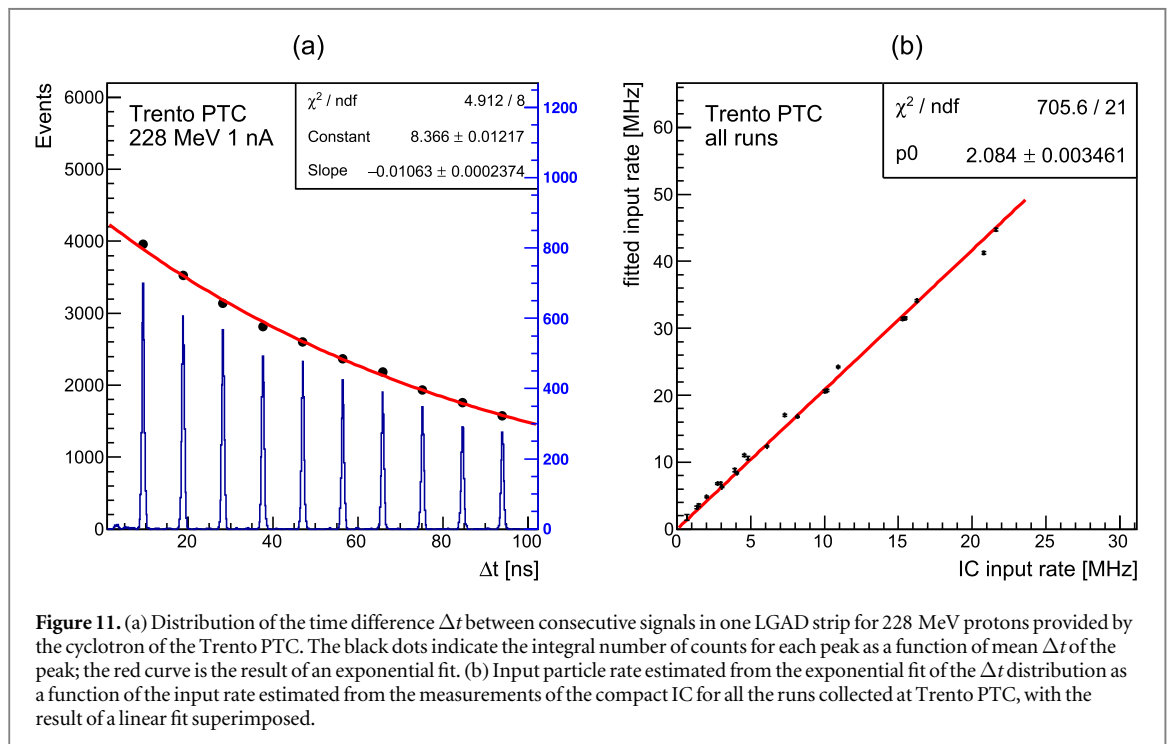
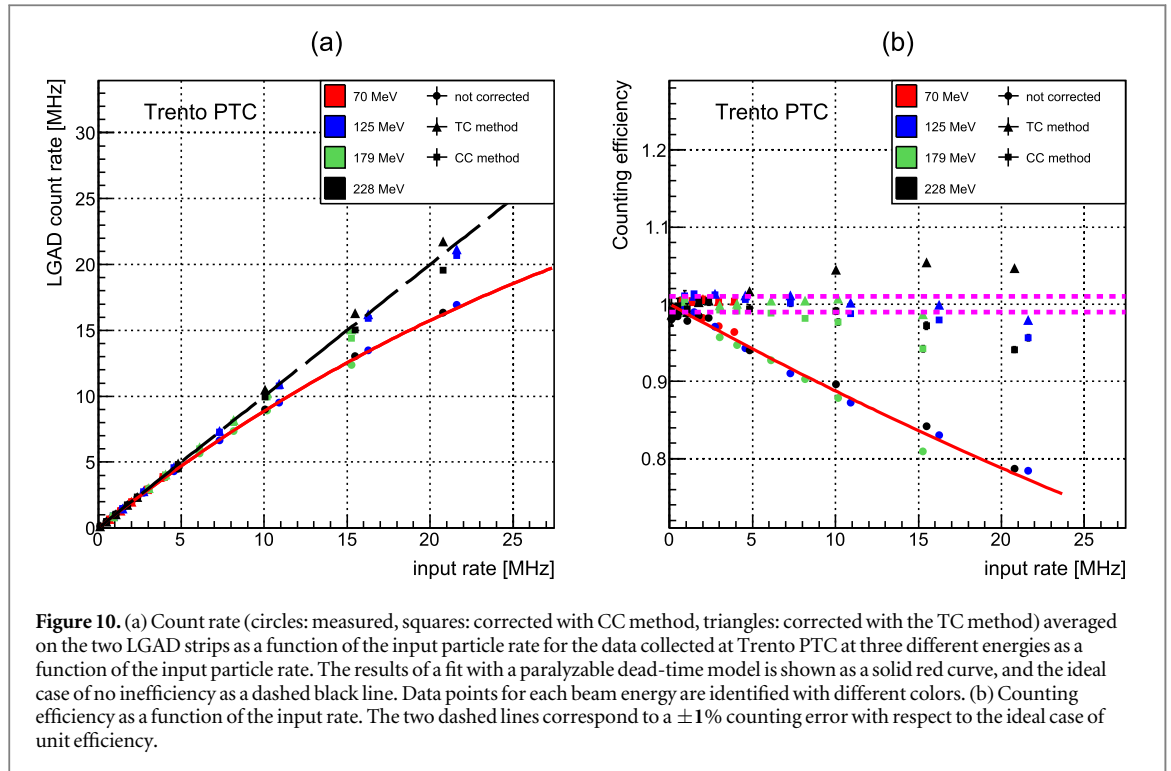
The main difference between the tests at CNAO and at the Trento PTC was the time structure of the proton beams (section 2.2), and the wider range in beam fluxes available at Trento; in particular at the Trento PTC it was possible to study the LGAD behavior at count rates below  $1 \text{ MHz strip}^{-1}$ , for which the strip sensors were designed.

The offline analysis of the data collected at the Trento PTC was performed following the same steps described in sections 3.1 and 3.2. The conversion of the LGAD counts and IC dose to counting and dose rates was performed using the duration of the whole irradiation period. A fitting of the count rates measured by the LGAD strip as a function of the dose rate measured by the IC through equations (3) and (7) was used to determine the C parameter needed to convert the IC dose rate into an estimate of the input particle rate on a strip for each energy.

The results corresponding to those reported for CNAO in figure 8 are now reported in figure 10. By comparison with figure 8, less fluctuations are found because of the more uniform beam conditions at the Trento PTC. The counting inefficiency without corrections was less than 1% up to  $1 \text{ MHz strip}^{-1}$ , corresponding to the design goal. After the application of the correction methods, almost all the points are within the  $\pm 1\%$  limits for all the energies up to  $8 \text{ MHz strip}^{-1}$  (corresponding to a fluence rate on a strip of about  $4 \times 10^8 \text{ p}/(\text{cm}^2 \cdot \text{s})$ ). The TC correction method overestimates the number of counts at higher energies and rates, where the time measurements are more difficult.

### 3.5. Study of the pulsed beam structure at the Trento proton therapy center

The distribution of the time interval  $\Delta t$  between consecutive signals in one strip was studied also with the data collected at the Trento PTC, to provide an independent estimation of the input particle rate, and validate the input rates based on the measurements from the compact IC.



An example of time interval distribution is shown in figure 11(a) for 228 MeV protons at an extraction current of 1 nA. The time interval distribution has several peaks, separated by 9.4 ns due to the beam structure of the IBA cyclotron (section 2.2). The number of events contributing to each peak is shown in the same figure with black dots as a function of the central  $\Delta t$  values of the peak, with the result of an exponential fit superimposed. The instantaneous input rate on a strip is estimated as the inverse of the exponential slope.

The relationship between the two independent estimations of the input particle rates is shown in figure 11(b), including all the runs acquired at the Trento PTC at different beam energies and extraction currents. The overlapped curve is the result of a linear fit with intercept forced to zero, which provides a slope

**Table 5.** Mean value of the pulse period, standard deviation of the time distribution of the irradiated pulses and effective dead times estimated after the corrections with the CC and TC methods for 4 different energies at the Trento PTC.

Energy (MeV)	Mean $\Delta t$ first peak (ns)	Std.dev. $\Delta t$ first peak (ns)	$\tau_{CC}$ (ns)	$\tau_{TC}$ (ns)
70	$9.34 \pm 0.01$	$1.405 \pm 0.006$	$10.0 \pm 0.6$	$11.3 \pm 0.9$
125	$9.383 \pm 0.003$	$0.962 \pm 0.002$	$10.0 \pm 1.0$	$12.0 \pm 1.0$
179	$9.396 \pm 0.002$	$0.656 \pm 0.001$	$9.8 \pm 0.4$	$13.8 \pm 0.5$
228	$9.396 \pm 0.001$	$0.342 \pm 0.001$	$8.7 \pm 0.5$	$15.1 \pm 0.5$

compatible with the expected factor 2 due to the 50% duty cycle of the beam time structure at the Trento PTC (section 2.2).

The first peaks of the  $\Delta t$  distributions were fitted by a Gaussians function and the corresponding mean and standard deviation values are reported in table 5, averaged over all the runs collected for each beam energy. The mean values are compatible with the expected period of the cyclotron radiofrequency (RF), while the increase of the standard deviation at lower beam energies reflects the effect of the degrader and energy selection system used to reduce the energy of the beam provided by the cyclotron. In table 5 the effective dead times  $\tau$  obtained by inverting equation (3) after the application of the CC a TC methods are also reported. The  $\tau$  values obtained by the CC method are compatible with the period of the cyclotron RF, as expected from equation (6), while those from the TC method are above the expectation, probably reflecting the overestimation of the corrected count rates in figure 10, especially at the highest energy.

#### 4. Discussion

The results of the tests of LGAD strip sensors with therapeutic proton beams demonstrate the possibility to discriminate and count the number of single beam particles with a maximum pile-up inefficiency of 1% at a count rate on a strip of 1 MHz, corresponding to a mean flux on the strip of about  $5 \times 10^7$  p/(cm<sup>2</sup>·s). This limit can be extended by almost one order of magnitude when dedicated pile-up mitigation algorithms are employed to correct for counting inefficiencies. These results were obtained irradiating the sensors with beams provided by a synchrotron at CNAO, and by a cyclotron at the Trento PTC. The time structure of the beam is different in the two cases: a bunched structure at CNAO and a pulsed irradiation at the Trento PTC. In both cases, the instantaneous particle flux is higher than the mean flux estimated with a compact IC, and therefore pile-up inefficiencies are higher than what can be expected based on the intrinsic dead time given by the signal duration. The results obtained at the Trento PTC are more solid than the ones from the test at CNAO, due to the wider choice of beam intensities, which allowed a more precise independent estimation of the input particle rates. Moreover, the results of the present study indicates a slight dependence of the bunch time structure of the CNAO beam on the degrader setting used to modulate the beam flux; this dependence influences the assumptions made to estimate the input rate from the measurements of the compact IC positioned close to the readout strips.

It is interesting how the duty-cycles of the particle bunches inside each spill at CNAO can be estimated from the count rates corrected for inefficiency effects. The instantaneous counting frequencies obtained from LGAD measurements are consistent with independent estimations from the exponential fittings of the distribution of the time intervals between consecutive particles.

At high beam energies and particle input rates, the two pile-up mitigation algorithms employed in this study start to fail in correcting counting inefficiencies. In particular, the TC mitigation method seems to overestimate the count rates and the effective dead times in such beam conditions. This is probably due to the lower signal-to-noise ratio of LGAD pulses at higher energies and to baseline instability at high beam fluxes, to which the time measurements used in the TC method are more sensitive in comparison with the CC method.

This work was intended as a proof-of-concept for the application of segmented solid-state devices to measure the beam fluence in therapeutic conditions, operating the device in single particle counting modality. The advantages with respect to the measurements with gas detectors are the higher sensitivity (ideally, each single beam particle can be detected), the faster response time (of the order of ns instead of hundreds of  $\mu$ s) and the possibility to provide measurements independent of calibrations, *a priori* knowledge of the beam energy and environmental conditions. The proposed technique could be useful as a calibration tool for beam monitoring devices, to check the beam time structure and, in the future, to develop innovative beam monitoring detectors able to operate at high speed for fast scanning delivery schemes or for high sensitive fluence measurements when a low number of particles are delivered to each spot.

In order to use a silicon detector as an online beam monitor in clinical treatment procedures, different issues must be addressed: radiation resistance, operation at therapeutic beam fluxes, large detector area, correction for detector geometrical acceptance and cost.

A source of concern is the radiation resistance of a silicon detector, because a device used in a clinical environment should be able to provide stable and solid results over a reasonable period. In particular, the irradiation of LGAD detectors de-activates the acceptors in the  $p^+$  implant and thus reduces the gain factor and the charge collection efficiency. The removal of the acceptors in the gain layer as a result of the radiation dose was intensively studied in the past years, in order to identify the design and manufacturing process which maximizes the radiation resistance (Jin *et al* 2020, Ferrero *et al* 2022). The best performance was obtained with 45  $\mu\text{m}$  thick sensors with boron as acceptor, an additional deep implant of carbons in the gain layer, and with an optimized annealing process to limit the diffusion of the implants. Sensors produced with this design were able to provide a reasonable gain factor and preserve a time resolution of 40 ps up to a fluence of  $2.5 \times 10^{15} \text{ n}_{\text{eq}} \text{ cm}^{-2}$  (Siviero *et al* 2022), corresponding to about one year of operation with a therapeutic proton beam. Further studies are ongoing to extend the radiation resistance of LGAD sensors to a fluence greater than  $10^{16} \text{ n}_{\text{eq}} \text{ cm}^{-2}$ , by using a compensated design of the gain implant (Sola *et al* 2022).

In addition to radiation damage, the irradiation of LGAD sensors produces an increase of the leakage current and, as a consequence, of the noise. This effect can be compensated by reducing the temperature of the sensor, as foreseen in high-energy physics applications. However, for a possible application of LGADs as a beam monitoring detector, a cooling system would add thickness and complexity. Therefore, the operation of the sensor at room temperature is desirable. The study described in this work will be extended in the future to investigate the performance of pre-irradiated LGAD detectors at room temperature to determine the maximum tolerable dose for their operation as beam particle counters.

A beam monitoring detector placed in the nozzle at the exit of the beam pipe, close to the patient, must have an area of at least  $20 \times 20 \text{ cm}^2$ . As an intermediate step toward this goal, dedicated LGAD strip detectors with an area of  $2.7 \times 2.7 \text{ cm}^2$  were produced by FBK, each one with 144 strips (Marti Villarreal (2023)). A dedicated 24-channel Application Specific Integrated Circuit (ASIC) chip was also developed by Torino University and INFN, implementing the electronics for the amplification and fast discrimination of the signals from each readout channel, able to operate up to 100 MHz/channel (Fausti *et al* 2021). The sensors and the ASIC are the core of a prototype beam monitoring device under development, where the output signals from the ASICs are processed by an FPGA, with no additional dead time from the pile-up correction algorithms. This prototype is still far from a full area detector covering the field side needed for beam monitoring in clinical practice, which will necessarily require the arrangement of smaller sensor elements in a reticle. For a  $20 \times 20 \text{ cm}^2$  strip detectors, each sensor element should have strips of about 10 cm length, has to be tiled on three sides, and connected to the readout electronics on the forth side. The high number of channels (of the order of a few thousands) requires high-density ASICs for the analog and digital readout electronics, to be placed out of the beam, possibly in a frame around the sensors. When the performance of the sensors degrades for the radiation dose, it is useful to foresee the mounting and bonding of new detectors inside the frame, without changing the electronics.

In this work, the count-loss for particles crossing the dead area between the two readout strips was neglected. A beam monitor device must be able to measure the total number of particles delivered to the patient, and therefore the particle counts from a segmented solid-state detector has to be corrected for a constant factor corresponding to the geometrical acceptance of the sensor. This correction should be a constant fraction for single regular structures. However, in case of large area LGAD panels composed by the arrangement of smaller sensors, the correction has to be position dependent to consider the dead area in the gaps between different detector elements. As an alternative, the single elements should have a periphery of very small dimensions to limit the dead regions between adjacent sensors.

Counting errors could also come from charge sharing effects between two adjacent channels, producing an overestimation of the number of discriminated signals. This effect was found to be negligible in the LGAD strip sensors used in this study, but must be taken into account in the design of alternative particle counting detectors.

Even with pile-up mitigation algorithm, the maximum count rate in strip detectors is limited by the strip area. Detectors with segmentation in smaller pixels are therefore needed to cope with therapeutic fluxes of  $10^9$  to  $10^{10} \text{ protons}/(\text{cm}^2 \cdot \text{s})$ .

The possibility of realizing large area pixelated LGAD detectors is demonstrated by the ongoing development of the timing layers of the ATLAS and CMS experiments at CERN (CMS Collaboration 2019, ATLAS Collaboration 2020), covering an area of the order of  $10 \text{ m}^2$ . These detectors must work for a considerable number of years in a harsh radiation environment, with integrated doses comparable or higher than those expected in one year of clinical irradiations with proton beams. The readout electronics is optimized for high temporal resolutions and not for particle counting at high rates, but the detector itself is a valuable possibility for large area beam monitoring silicon panels.



In general, even if silicon detectors have several advantages in comparison to traditional gas detectors in particle beam monitoring applications, they are more complex and require higher production costs. Also the maintenance of the detector is more expensive, due to the need to replace the sensors periodically.

A more cost-effective solution could be based on DMAPS sensors manufactured with standard CMOS technology (Braach *et al* 2022, Dierlamm *et al* 2023). In comparison to hybrid detectors where the active sensor is bump bonded to a readout chip, in monolithic detectors the electronics and the sensitive region are embedded in the same chip, reducing the total thicknesses, the space for the connection to the external electronics, and the total cost. The LGAD technology has already been implemented in CMOS DMAPS, providing excellent position and timing resolutions (Iacobucci *et al* 2021).

The development of large area LGAD panels is also of interest for other medical applications, for example for time-of-flight measurement of the proton energy in a telescope of LGAD detectors for beam energy verification (Vignati *et al* 2020) or for proton computed tomography applications (Ulrich-Pur *et al* 2022). Another possible application is to provide a time trigger for range verification in particle therapy with prompt-gamma timing technique (Pennazio *et al* 2022).

## 5. Conclusions

The performance of LGAD sensors segmented in strips and operated in particle counting mode was studied in realistic therapeutic environments, to investigate the potentiality of the LGAD technology for beam characterization and monitoring applications in particle therapy. The possibility to discriminate single beam protons and count their number is demonstrated for beam mean fluxes on a strip up to  $5 \times 10^7$  p/(cm<sup>2</sup>·s), above which the counting inefficiency due to pile-up effects is greater than 1%. This limit in flux can be extended to about  $4 \times 10^8$  p/(cm<sup>2</sup>·s) by applying pile-up mitigation algorithms based on logic combinations of signals from two nearby strips. The study was performed with protons provided by a cyclotron and a synchrotron, with different beam time structures but with similar results in terms of counting efficiency as a function of the beam flux. It is also demonstrated how information on the instantaneous particle rate and on the beam structure can be obtained using only the counts from the detector strips.

The direct counting of beam protons opens the way to further developments, which could lead to innovative devices to monitor the flux and position of proton pencil beams, with enhanced sensitivity, higher response speed and independence of calibration procedures, in the optics to provide tools for advanced delivery techniques and to improve the precision and effectiveness of particle therapy.

## Acknowledgments

This work was financed by INFN CSN5 (MoveIT project) and supported by European Union's Horizon 2020 Research and Innovation funding program (ERC UFSD669529) and Ministero della Ricerca, PRIN 2017, project '4DInsiDe' (MIUR PRIN 2017L2XKTJ). We kindly acknowledge the dedicated collaboration of FBK and the UFSD group, and the key contributions of the irradiation facilities of CNAO and Trento Proton Therapy Center.

## Data availability statement

All data that support the findings of this study are included within the article (and any supplementary information files).

## Ethical statement

This research does not contain any studies with human or animal subjects. Therefore, ethical approval is not applicable for this article.


## ORCID iDs

Vincenzo Monaco  <https://orcid.org/0000-0002-3617-2432>

Omar Hammad Ali  <https://orcid.org/0000-0001-6294-8233>

Davide Bersani  <https://orcid.org/0009-0007-3773-4699>

Mohammed Abujami  <https://orcid.org/0000-0001-6228-7738>

Maurizio Boscardin  <https://orcid.org/0000-0002-0052-5793>

Nicolò Cartiglia [ORCID](https://orcid.org/0000-0002-0548-9189) <https://orcid.org/0000-0002-0548-9189>  
Gian Franco Dalla Betta [ORCID](https://orcid.org/0000-0001-5516-9282) <https://orcid.org/0000-0001-5516-9282>  
Emanuele Data [ORCID](https://orcid.org/0009-0002-1351-1523) <https://orcid.org/0009-0002-1351-1523>  
Marco Donetti [ORCID](https://orcid.org/0000-0001-7489-6274) <https://orcid.org/0000-0001-7489-6274>  
Marco Ferrero [ORCID](https://orcid.org/0000-0001-9676-8222) <https://orcid.org/0000-0001-9676-8222>  
Francesco Ficorella [ORCID](https://orcid.org/0000-0002-0296-1193) <https://orcid.org/0000-0002-0296-1193>  
Simona Giordanengo [ORCID](https://orcid.org/0000-0001-6347-1182) <https://orcid.org/0000-0001-6347-1182>  
Oscar Ariel Marti Villarreal [ORCID](https://orcid.org/0000-0003-2083-9797) <https://orcid.org/0000-0003-2083-9797>  
Felix Mas Milian [ORCID](https://orcid.org/0000-0002-5588-1672) <https://orcid.org/0000-0002-5588-1672>  
Mohammad-Reza Mohammadian-Behbahani [ORCID](https://orcid.org/0000-0002-8160-6148) <https://orcid.org/0000-0002-8160-6148>  
Diango Montalvan Olivares [ORCID](https://orcid.org/0000-0002-3733-2899) <https://orcid.org/0000-0002-3733-2899>  
Marco Pullia [ORCID](https://orcid.org/0000-0003-1851-431X) <https://orcid.org/0000-0003-1851-431X>  
Francesco Tommasino [ORCID](https://orcid.org/0000-0002-8684-9261) <https://orcid.org/0000-0002-8684-9261>  
Enrico Verroi [ORCID](https://orcid.org/0000-0003-0957-4505) <https://orcid.org/0000-0003-0957-4505>  
Anna Vignati [ORCID](https://orcid.org/0000-0001-8137-9080) <https://orcid.org/0000-0001-8137-9080>  
Roberto Cirio [ORCID](https://orcid.org/0000-0001-9669-848X) <https://orcid.org/0000-0001-9669-848X>  
Roberto Sacchi [ORCID](https://orcid.org/0000-0001-7794-0170) <https://orcid.org/0000-0001-7794-0170>

## References

- Altieri *et al* 2018 A beam monitor based on MPGD detectors for hadron therapy *EPJ Web Conf.* **174** 01011
- ATLAS Collaboration 2020 Technical design report: a high-granularity timing detector for the ATLAS Phase-II upgrade CERN-LHCC-2020-007 ATLAS-TDR-031 (<https://cds.cern.ch/record/2719855?ln=itCMS>)
- Braach J *et al* 2022 Performance of the FASTPIX sub-nanosecond CMOS pixel sensor demonstrator *Instruments* **6** 13
- Cartiglia N *et al* 2022 4D tracking: present status and perspectives *Nucl. Instr. Meth. A* **1040** 167228
- CMS Collaboration 2019 Technical Design Report: A MIP Timing Detector for the CMS Phase-2 Upgrade CERN-LHCC-2019-003 CMS-TDR-020 (<https://cds.cern.ch/record/2667167?ln=it>)
- Combs S E *et al* 2010 Particle therapy at the Heidelberg Ion therapy center (HIT)—integrated research-driven university-hospital-based radiation oncology service in Heidelberg, Germany *Radioth. Oncol.* **95** 41–4
- Courtois C *et al* 2014 Characterization and performances of a monitoring ionization chamber dedicated to IBA-universal irradiation head for pencil beam scanning *Nucl. Instrum. Meth. A* **736** 112–7
- Coutrakon M *et al* 1991 A prototype beam delivery system for the proton medical accelerator at Loma Linda *Med. Phys.* **18** 1093–9
- Dierlamm A *et al* 2023 A beam monitor for ion beam therapy based on HV-CMOS pixel detectors *Instruments* **7** 9
- Durante M *et al* 2017 Charged-particle therapy in cancer: clinical uses and future perspectives *Nat. Rev. Clin. Oncol.* **14** 483–95
- Fausti F *et al* 2021 A single ion discriminator ASIC prototype for particle therapy applications *Nucl. Instr. Meth. A* **985** 164666
- Ferrero M *et al* 2019 Radiation resistant LGAD design *Nucl. Instrum. Meth. A* **919** 16–26
- Ferrero M *et al* 2022 Radiation resistant LGAD design *Nucl. Instrum. Meth. A* **1040** 167232
- Flynn S *et al* 2022 Monitoring pencil beam scanned proton radiotherapy using a large format CMOS detector *Nucl. Instr. Meth. A* **1033** 166703
- Giordanengo S *et al* 2013 Design and characterization of the beam monitor detectors of the Italian National Center of Oncological Hadron-therapy (CNAO) *Nucl. Instrum. Meth. A* **698** 202–7
- Giordanengo S *et al* 2015 The CNAO dose delivery system for modulated scanning ion beam radiotherapy *Med. Phys.* **42** 263–75
- Haberer T *et al* 1993 Magnetic scanning system for heavy ion therapy *Nucl. Instrum. Meth. A* **330** 296–305
- Hoffmann A *et al* 2020 MR-guided proton therapy: a review and a preview *Radiat. Oncol.* **15** 129
- Iacobucci G *et al* 2021 Monolithic picosecond silicon pixel sensors for future physics: experiments and applications *IEEE Instrum. Meas. Mag.* **24** 5–11
- Jin J *et al* 2020 Experimental study of acceptor removal in UFSD *Nucl. Instr. Meth. A* **983** 164611
- Klimpki G *et al* 2018 The impact of pencil beam scanning techniques on the effectiveness and efficiency of rescanning moving targets *Phys. Med. Biol.* **63** 145006
- Knoll G F 2010 *Radiation detection and measurement* (New York: John Wiley & Sons) 4th edn
- Leverington *et al* 2018 A prototype scintillating fibre beam profile monitor for Ion therapy beams *JINST* **13** P05030
- Lin S *et al* 2009 More than 10 years experience of beam monitoring with the Gantry 1 spot scanning proton therapy facility at PSI *Med. Phys.* **36** 5331–40
- Loeffler J S *et al* 2013 Charged particle therapy—optimization, challenges and future directions *Nat. Rev. Clin. Oncol.* **10** 411–24
- Lomax A 1999 Intensity modulation methods for proton radiotherapy *Phys. Med. Biol.* **44** 185
- Lomax A *et al* 2004 The clinical potential of intensity modulated proton therapy *Z. Med. Phys.* **14** 147–52
- Marti Villarreal O A *et al* 2023 Characterization of thin LGAD sensors designed for beam monitoring in proton therapy *Nucl. Instrum. Meth. A* **1046** 167622
- Martišiková M *et al* 2011 Test of an amorphous silicon detector in medical proton beams *Nucl. Instr. Meth. A* **633** S259–61
- Matsumoto Y *et al* 2021 A critical review of radiation therapy: from particle beam therapy (Proton, Carbon, and BNCT) to beyond *J. Pers. Med.* **11** 825
- Mirandola A *et al* 2015 Dosimetric commissioning and quality assurance of scanned ion beams at the Italian national center for oncological hadrontherapy *Med. Phys.* **42** 5287–300
- Mohammadian-Behbahani M *et al* 2022 Two-channel combination methods for count-loss correction in radiation measurements at high rates and with pulsed sources *Nucl. Instrum. Meth. A* **1040** 167195
- Paganetti H *et al* 2018 *Proton Therapy Physics (NY)* 2nd edn (CRC Press)
- Pellegrini G *et al* 2014 Technology developments and first measurements of low gain avalanche detectors (LGAD) for high energy physics applications *Nucl. Instrum. Meth. A* **765** 12–6

- Pennazio F *et al* 2022 Proton therapy monitoring: spatiotemporal emission reconstruction with prompt gamma timing and implementation with PET detectors *Phys. Med. Biol.* **67** 065005
- Radhe M 2022 A review of proton therapy—current status and future directions *Prec. Radiat. Oncol.* **6** 164–76
- Sadrozinski H F W *et al* 2018 4-dimensional tracking with ultra-fast silicon detectors *Rep. Progress Phys.* **81** 026101
- Sauli F 1997 GEM: a new concept for electron amplification in gas detectors *Nucl. Instr. Meth. A* **386** 531
- Siviero F *et al* 2022 Optimization of the gain layer design of ultra-fast silicon detectors *Nucl. Instr. Meth. A* **1033** 166739
- Sola V *et al* 2019 First FBK production of 50  $\mu\text{m}$  ultra-fast silicon detectors *Nucl. Instrum. Meth. A* **924** 360–8
- Sola V *et al* 2022 A compensated design of the LGAD gain layer *Nucl. Instrum. Meth. A* **1040** 167232
- Terakawa *et al* 2015 A micro-pattern gaseous detector for beam monitoring in ion-therapy *Nucl. Instrum. Meth. B* **365** 606–10
- Tommasino F *et al* 2017 Proton beam characterization in the experimental room of the trento proton therapy facility *Nucl. Instrum. Meth. A* **869** 15–20
- Ulrich-Pur F *et al* 2022 Feasibility study of a proton CT system based on 4D-tracking and residual energy determination via time-of-flight *Phys. Med. Biol.* **67** 095005
- Vignati A *et al* 2020 A new detector for the beam energy measurement in proton therapy: a feasibility study *Phys. Med. Biol.* **65** 215030
- Yang Y *et al* 2022 A 2D strip ionization chamber array with high spatiotemporal resolution for proton pencil beam scanning FLASH radiotherapy *Med. Phys.* **49** 5464–75
- Yap J S L *et al* 2021 Medipix3 for dosimetry and real-time beam monitoring: first tests at a 60 MeV proton therapy facility *JINST* **16** T11001